Authors' final copy; accepted @ EPSL Jan. 2019

Paired organic matter and pyrite $\delta^{34}S$ records reveal mechanisms of carbon, sulfur, and iron cycle disruption during Ocean Anoxic Event 2

Morgan Reed Raven[*a,b], David A. Fike [b], Alexander S. Bradley [b]; Maya L. Gomes [c],
Jeremy D. Owens [d], Samuel A. Webb [e]

[a] Dept. of Earth Sciences, University of California, Santa Barbara, CA 93130 USA
[b] Dept. of Earth and Planetary Sciences, Washington University in St Louis, MO 63130
[c] Dept. of Earth and Planetary Sciences, Johns Hopkins University, Baltimore, MD 21218
[d] Dept. of Earth, Ocean, and Atmospheric Science, Florida State University, Tallahassee, FL 32306
[e] Stanford Synchrotron Radiation Lightsource, Stanford University, Menlo Park, CA, 94025
* = *corresponding author, raven@ucsb.edu*

Abstract

The sulfur (S) isotope composition of pyrite in the sedimentary record has played an important part in our understanding of the evolution of biogeochemical cycles throughout Earth history. However, the kinetics of pyritization are complex and depend strongly on the reactivity and mineralogy of available iron. As a second major sink for sulfide in anoxic sediments, organic matter (OM) provides essential context for reconstructing the distribution and isotopic composition of environmental sulfide. To first order, roughly parallel pyrite and OM $\delta^{34}S$ profiles reflect changes in sulfide, while independent patterns require alternative explanations, including changes in iron availability or OM characteristics. We apply this framework to Ocean Anoxic Event 2 (OAE-2, ~94 Mya), a period of enhanced burial of reduced C and S (in OM and pyrite) that has been associated with an expansion of reducing marine conditions. We present paired S-isotope records for pyrite and OM along with profiles of OM S:C ratio and S redox speciation from four well-characterized lithologic sections with a range of depositional environments (Pont d'Issole, Cismon, Tarfaya Basin, and Demerara Rise) to reconstruct both local redox structure and global mechanisms impacting the C, S and Fe cycles around OAE-2.

OM sulfurization appears to be a major control on OM preservation at all four sites. Similar to modern anoxic environments, there is a positive correlation between OM S:C ratios and TOC concentrations for sites with more reducing conditions, implying a link between OM sulfurization and burial. At consistently anoxic sites like Tarfaya Basin and Demerara Rise, strongly sulfurized OM with a consistent S redox speciation and S-isotope composition most likely formed rapidly in sinking particles before, during, and after OAE-2. Particle-hosted OM sulfurization may therefore have been a central mechanism facilitating the massive burial of OM in anoxic environments during this and other periods of enhanced global carbon burial. At the same time, a nearly 25‰ negative shift in the δ^{34}S values of pyrite – but not OM – occurs at multiple, globally distributed sites prior to the onset of OAE-2, indicating slower pyritization reactions that likely reflect changes in iron delivery due to expanding regional or global anoxia. The combination of pyrite and organic S isotopes thus provides novel constraints on the interwoven cycles of carbon, iron, and sulfur across a major carbon cycle perturbation.

1. Introduction

Ocean Anoxic Event 2 (OAE-2, also termed the Cenomanian–Turonian Boundary Event) was a period of dynamic changes in the global carbon cycle in the Cretaceous (~94 million years ago, Mya) during which a large portion of the global ocean experienced anoxia (Ostrander et al., 2017) and associated biological turnover (Keller et al., 2008 and refs therein). Expanded euxinia at the onset of the event contributed to the preservation of extraordinary amounts of organic matter (OM) in marine sediments, equivalent to roughly a 60 to 80% increase in the global organic carbon burial flux maintained for ~500,000 years (Owens et al., 2013; 2018; Sageman et al., 2006). This burst of ^{13}C-depleted OM preservation generated the characteristic positive C-isotope excursion for OAE-2 and substantially drew down atmospheric CO_2 (Jarvis et al., 2011). OM sulfurization can enhance the preservation of total organic carbon (TOC) under anoxic conditions (Boussafir et al., 1995) and has been described in TOC–rich (>10 wt%) OAE-2 shales (Hetzel et al., 2009; Kolonic et al., 2002) as well as in interbedded carbonates and marly shales with more moderate (0.2–3 wt%) TOC (Raven et al., 2018). Still, it remains difficult to quantify the impact of sulfurization on OM preservation under different environmental conditions, much less to extrapolate to global fluxes of reduced sulfur and carbon burial or to estimate how those fluxes might change before, during, and after OAE-2.

Primary considerations for determining the significance of sulfurization for TOC burial are the rates and locations of S cycling in the environment. Two distinct timescales of sulfurization reactions occur in modern environments: gradual sulfurization reactions between bisulfide (HS^{-}) and relatively recalcitrant OM occur over thousands of years under strongly reducing conditions (Werne et al., 2000), and rapid sulfurization reactions between polysulfides (S_x^{2-}) and relatively fresh, labile OM occur on timescales of days near dynamic redox interfaces, for example in sinking marine particles (Raven et al., 2016a). Rapid sulfurization has the potential to have a much more dramatic impact on TOC burial because it can compete with microbial heterotrophy and preserve part of the relatively large pool of fresh OM sinking out of the surface ocean (Raven et al., 2018). Still, particle-hosted OM sulfurization has not been explicitly considered in analyses of TOC and sulfur burial during periods of expanded oceanic anoxia like OAE-2.

Sulfur–isotope ratios (expressed as $\delta^{34}S$ values) are powerful tools for reconstructing the sources of sulfide in the environment as well as its various potential sinks, including reoxidation or precipitation as either abiogenic organic S or pyrite (FeS_2). Near the onset of OAE-2, previously published S-isotope profiles of pyrite from multiple sites show intriguing shifts toward ^{34}S-depleted values that have been interpreted in terms of changing marine sulfate concentrations (Adams et al., 2010), local chemocline position (Gomes et al., 2016), and the extent of oxidative microbial sulfur cycling (Hetzel et al., 2009; Kolonic et al., 2002). Although each of these hypotheses invoke changes in the distribution or $\delta^{34}S$ value of sulfide in the environment, OAE-2 is also associated with major changes in iron cycling due to inputs from active rifting and volcanism (Owens et al., 2012), which could also impact pyrite $\delta^{34}S$ values via changes in iron distributions and mineralogy. If changes in the distribution or isotopic composition of sulfide are driving the shift in pyrite $\delta^{34}S$ values near the onset of OAE-2, we should see parallel behavior in the $\delta^{34}S$ values of sulfurized OM and pyrite. If not, changes in pyrite $\delta^{34}S$ values may instead reflect changes in the quantity and/or speciation of locally available iron at this time, which could impact the mechanism and timing of pyrite formation in the environment.

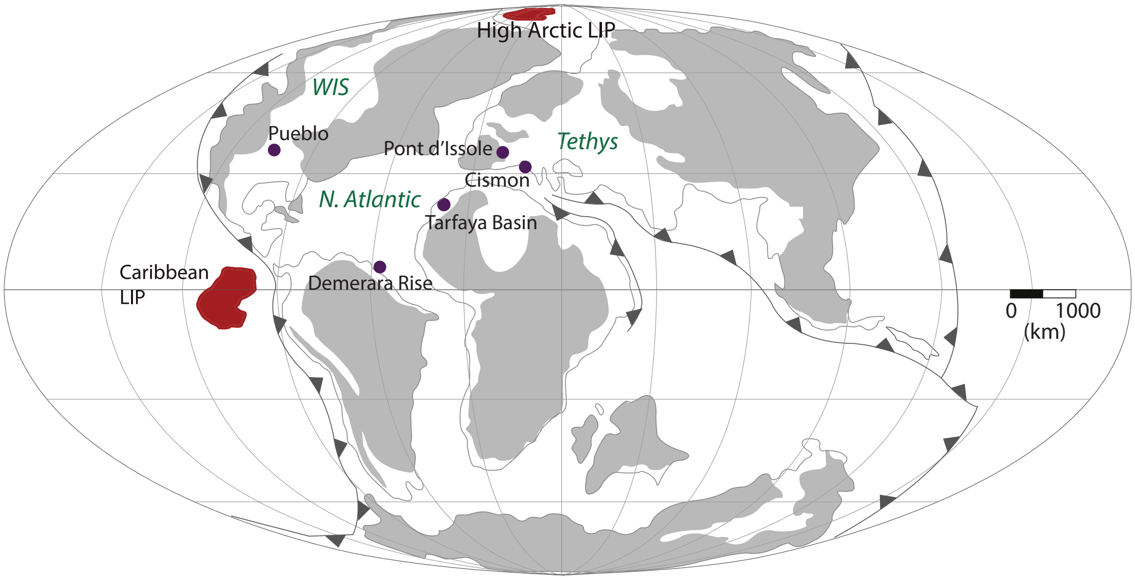

Fig. 1 Paleo-geography of study sites during OAE-2. Map is modified from du Vivier et al. (2014) with study sections marked by purple circles. Locations of Large Igneous Provinces (LIP) are also shown in red.

To distinguish among these possible drivers of S-isotope variability, we present paired pyrite and OM δ^{34}S records alongside OM S speciation data for four OAE-2 sections located in different regions of the Tethys and proto–North Atlantic Oceans (Fig. 1). Results for organic S from Pont d'Issole were previously published (Raven et al., 2018); all other data are new to this study. Our results indicate that the strong negative shift in pyrite δ^{34}S values from globally dispersed sites likely reflects a change in the quantity or speciation of iron delivery to these locations. We also find evidence for a generalizable relationship between sulfurization intensity and OM preservation in sediments, which implies that OM sulfurization can be a primary driver of changes in C burial during OAE-2 and throughout the Phanerozoic.

2. Brief Methods

Samples were prepared from previously sampled sections (see descriptions in Results) by sequential extraction (Canfield et al., 1986; Raven et al., 2018), as detailed in the Supplementary Information. Powdered rock samples were washed with deionized water, lyophilized, and microwave–extracted to remove organic-solvent soluble S, including any elemental S. Solids were weighed before and after acidification to estimate carbonate mineral ('carbonate') abundance. Pyrite in the carbonate-free sediments was extracted by treatment with hot chromium (II) chloride solution and the released sulfide, which we refer to as 'pyrite', was trapped as ZnS. Washed ZnS solids were oxidized to sulfate, quantified by ion chromatography, and precipitated as $BaSO_4$ for S-isotope analysis. Remaining solids after chromium reduction are considered 'organic S'. All C- and S-isotope ratio measurements were made by combustion EA-IRMS at Washington University in St Louis and are reported in per mil (‰) units relative to VPDB and VCDT, respectively (see Supplementary Information for analytical details). Error bars on Figures (±0.5‰ for $\delta^{34}S$ and ±0.2‰ for $\delta^{13}C$) represent typical standard deviations of results for external replicates (separately processed sample splits; n≥3). To determine the bonding environment of organic S, extracted sediments were analyzed by x-ray absorption spectroscopy on beamline 14–3 at the Stanford Synchrotron Radiation Lightsource (SSRL) at the SLAC National Accelerator Laboratory (see Supplementary Information).

3. Study Sites and Results

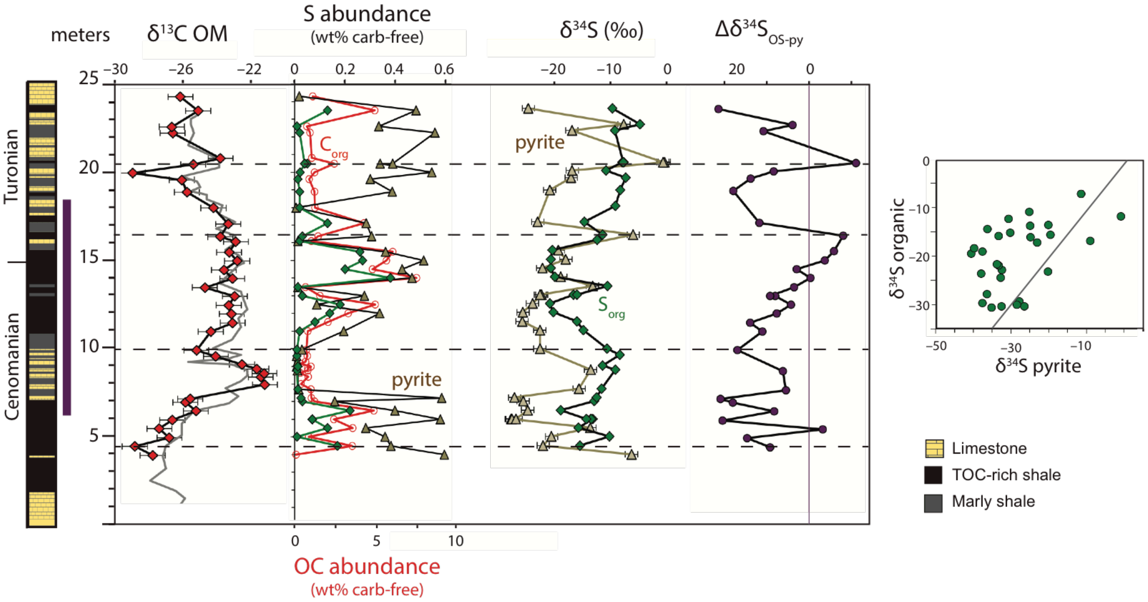

Fig. 2 Pont d'Issole record. The purple bar at left represents the interpreted duration of OAE-2 based on the C-isotope excursion. The grey line for $\delta^{13}C_{OM}$ is from Jarvis et al. (2011), and lithology is from Gomes et al. (2016). Dashed horizontal lines are intended as

visual aids to highlight patterns in the records. Vertical purple line for $\Delta\delta^{34}S_{OS\text{-}py}$ shows $\delta^{34}S_{pyrite} = \delta^{34}S_{OS}$. Grey line in the right-hand panel shows a 1:1 line.

The Pont d'Issole section was deposited in a subsiding basin within the northern Tethys Ocean (~30°N, Fig. 1) in several hundred meters of water depth with an average sedimentation rate of roughly 2.4 cm/yr (based on a 12-m-thick C-isotope excursion spanning ~500 kyr; Jarvis et al., 2011). Samples were collected at outcrop in 2011. A selection of mostly OM-lean carbonates from this section were analyzed previously for S-isotopes in pyrite and carbonate-associated sulfate (Gomes et al., 2016). The Pont d'Issole section is characterized by recurrent shifts in lithology and OM concentration between relatively TOC-lean (<0.2 wt%) limestones and relatively TOC-rich (>1.0 wt%) shales and marly shales. Our pyrite $\delta^{34}S$ profile from Pont d'Issole (Fig. 2) has many similarities to the published OM $\delta^{34}S$ profile (Raven et al., 2018), with comparable shifts toward lower $\delta^{34}S$ values in shales before and during the OAE-2 C-isotope excursion. There are also instances, however, where the S-isotope composition of pyrite behaves independently from that of OM: at 5.5 m and 20.5 m, for example, pyrite is locally strongly ^{34}S-enriched without any parallel excursion in OM $\delta^{34}S$. Additionally, the $\delta^{34}S$ offset between pyrite and organic matter (Fig. 2, $\Delta\delta^{34}S_{OS\text{-}py}$) decreases systematically across the duration of the C-isotope excursion from 17.4‰, a large but not unusual ^{34}S-enrichment for OM relative to pyrite, to –7.9‰, meaning that the normal relationship between pyrite and OM $\delta^{34}S$ values is reversed, with OM more ^{34}S-depleted than pyrite (Anderson and Pratt, 1995). Illustrating the variability in $\Delta\delta^{34}S_{OS\text{-}py}$ at Pont d'Issole, OM and pyrite $\delta^{34}S$ values show significant spread around and to the left of the 1:1 line in the cross-plot in Fig. 2.

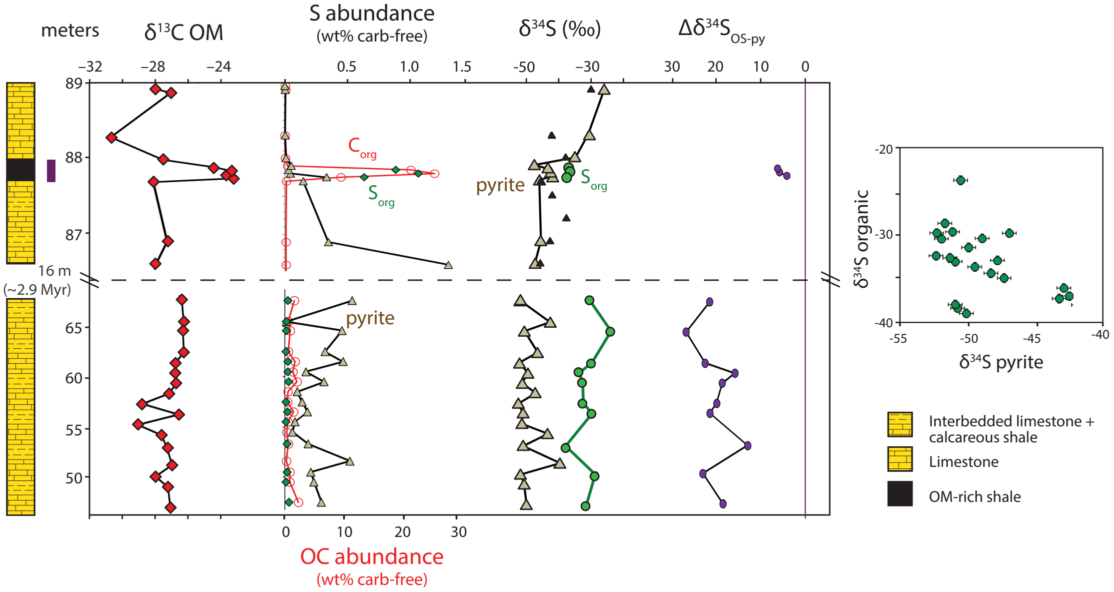

Fig. 3 Cismon record. The purple bar at left represents the interpreted duration of OAE-2 based on the C-isotope excursion. The horizontal dashed line indicates a 16-m gap in the vertical profile comprising very TOC-lean carbonates; note different scales for the upper and lower panels. The duration of this gap is ~2.9 Myr based on foraminiferal biozones, with an uncertainty of ±0.55 My for each stratigraphic interval (Bellanca et al., 1996; Gambacorta et al., 2015). Lithology and published pyrite data (black triangles) are from Gomes et al. (2016). Vertical purple line for $\Delta\delta^{34}S_{OS\text{-}py}$ shows $\delta^{34}S_{pyrite} = \delta^{34}S_{OS}$.

At Cismon, a narrow, ~35-cm-thick layer of TOC-rich (6.5 – 21.4 wt%) black shale corresponds to part of the OAE-2 C-isotope excursion, although major portions of the C-isotope excursion are absent due to hiatuses (Gambacorta et al., 2015; Gomes et al., 2016). On either side of this lithologic unit, corresponding to the Bonarelli Layer, rocks from Cismon are bedded layers of TOC-lean (≤ 0.05 wt%), micritic foraminiferal limestones with occasional cherts and grey shales (Bellanca et al., 1996; Gambacorta et al., 2015).

Pyrite and carbonate-associated sulfate $\delta^{34}S$ values for a subset of the samples collected at outcrop in 2011 were previously published for a subset of mostly TOC-lean carbonates in the upper portion of the study interval (Gomes et al., 2016, Fig. 3). Here, we expand on that record and add OM $\delta^{34}S$ values where possible. Unfortunately, the limestones immediately surrounding the black shale unit are generally too TOC-lean and silicate-rich to permit spectroscopic analysis of S speciation or isotopic analysis of organic S by conventional EA-IRMS. For a point of comparison with OAE-2 shales, we analyzed a selection of limestones with 0.1–0.7 wt% TOC from lower in the section, representing approximately 96 – 100 Mya (spanning a 20-meter-thick zone from 37.5 m above the OAE-1a C-isotope excursion to 20 m below the onset of OAE-2, Fig. 3). In both the TOC-rich layer and earlier TOC-lean limestones, OM from Cismon is strongly ^{34}S-depleted, with $\delta^{34}S$ values averaging –37‰ during OAE-2 and –38.8‰ in the earlier samples. Pyrite is strongly ^{34}S-depleted in the deeper, moderately TOC-rich carbonates and somewhat less so in the black shale unit; pyrite $\delta^{34}S$ values for these lithologies average –49‰ and –42.7‰, respectively. The difference between the $\delta^{34}S$ values of pyrite and OM ($\Delta\delta^{34}S_{OS-py}$) averages 20.3‰ in the deeper carbonates but only 5.4‰ in the black shale.

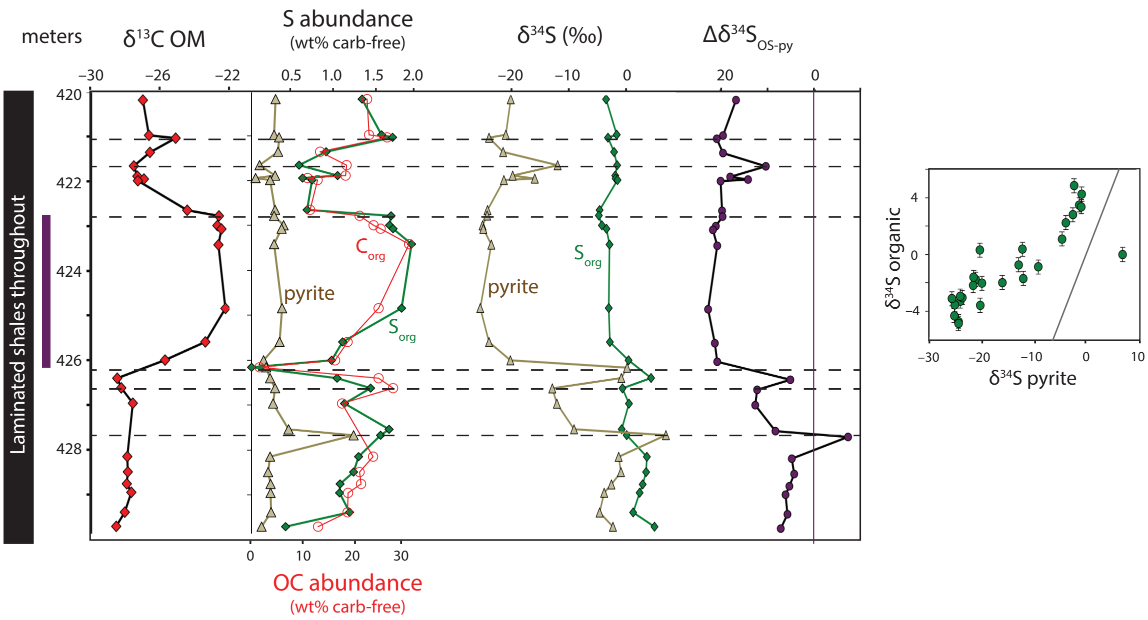

Fig. 4 Demerara Rise record. The purple bar at left represents the interpreted duration of OAE-2 based on the C-isotope excursion. Dashed horizontal lines are intended as visual aids to highlight patterns in the records. Vertical purple line for $\Delta\delta^{34}S_{OS\text{-}py}$ shows $\delta^{34}S_{pyrite} = \delta^{34}S_{OS}$. Grey line in the right-hand panel shows a 1:1 line.

Sediments from Demerara Rise were deposited in the western tropical proto-North Atlantic Ocean and were sampled as part of Ocean Drilling Program Leg 207 (Site 1258). Sediments throughout the investigated section (with modified composite depths after Erbacher et al., 2005) are generally described as laminated TOC-rich marl to black shales, with an apparent average sedimentation rate of ~0.8 cm/kyr for the 4.0-m-thick C-isotope excursion (Owens et al., 2016). On a carbonate-free basis, concentrations of TOC, organic S, and pyrite S show no large-scale trends across the onset and termination of the OAE (Fig. 4; Owens et al., 2016). Due to reduced carbonate concentrations during the C-isotope excursion, there is a perceived increase in pyrite and TOC concentrations across this interval on a whole-rock basis (Hetzel et al., 2009). Sediments are extremely OM-rich (Erbacher et al., 2005; Hetzel et al., 2009), containing an average of 24 wt% TOC (Fig. 4; Owens et al., 2016) and 4.1 wt% organic S on a carbonate-free basis. These concentrations of organic S exceed those of pyrite S by roughly five times. Organic matter $\delta^{34}S$ values are far less variable than pyrite values; although samples after the onset of the OAE are slightly more ^{34}S-depleted, all OM $\delta^{34}S$ values fall in a relatively narrow range between –4.9‰ and +4.8‰. In contrast, pyrite $\delta^{34}S$ values decline substantially across the 2 meters of section prior to the onset of OAE-2, from approximately –3‰ to–25‰, consistent with Hetzel et al. (2009). Pyrite S-isotopes are relatively stable at these moderately ^{34}S-depleted compositions throughout the OAE-2 C-isotope excursion and recover partly after the termination of the event. Accordingly, $\Delta\delta^{34}S_{OS\text{-}py}$ at Demerara Rise increases from ~6‰ prior to OAE-2 to ~21‰ during the OAE-2 C-isotope excursion, and the slope of the data in a pyrite–OM $\delta^{34}S$ crossplot is much shallower than the 1:1 line. Like at Pont d'Issole, there are also instances of locally ^{34}S-enriched pyrite in a sample without similar enrichment in organic S (e.g., 427.7 m).

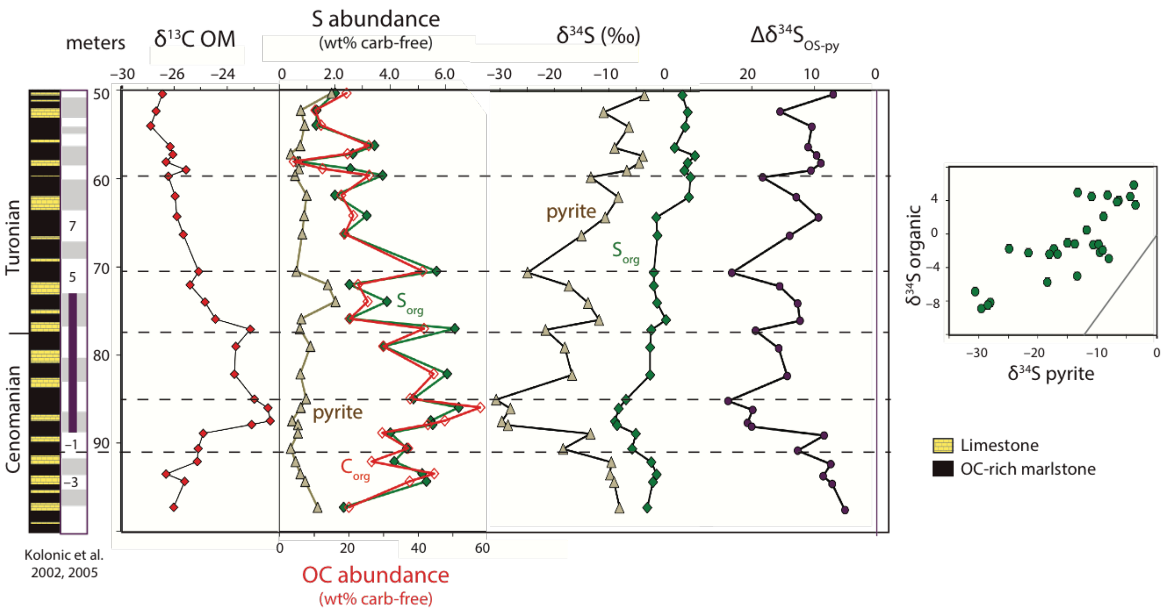

Fig. 5 Tarfaya Basin record. Lithology is shown at left, paired with recurrent sedimentary cycles from Kolonic (2002, 2005). Dashed horizontal lines indicate depths with relatively abundant OM and ^{34}S-depleted pyrite. The purple bar at left represents the interpreted duration of OAE-2 based on the C-isotope excursion. Vertical purple line for $\Delta\delta^{34}S_{OS\text{-}py}$ shows $\delta^{34}S_{pyrite} = \delta^{34}S_{OS}$. Grey line in the right-hand panel shows a 1:1 line.

Tarfaya Basin sediments (sampled from Shell exploration core S75) were deposited on the outer shelf of northwest Africa during a series of transgressive cycles associated with rifting of the southern North Atlantic Basin. High productivity and high sedimentation rates (averaging ~3.3 cm/kyr across the 16.5-meter-thick C-isotope excursion; Kolonic et al., 2005) supported the formation of extremely TOC-rich black shales and somewhat less TOC-rich carbonates, which alternate on apparently orbital timescales (Kolonic et al., 2005; 2002; Poulton et al., 2015; Fig. 5). This variation is also apparent in the δ^{34}S profile of pyrite, which is consistent with lower resolution data from Kolonic et al. (2002) and

Böttcher et al. (unpublished) as reported in Hetzel et al. (2009). Although we do not have the sampling density to resolve individual orbital cycles, TOC-rich layers generally contain relatively ^{34}S-depleted pyrite, as highlighted in dashed lines in Fig. 5. On top of this regular variation, the S-isotope profiles for TOC and pyrite have key similarities to those from Demerara Rise. TOC and pyrite δ^{34}S values prior to the onset of the OAE are between 0 and –10‰. By the onset of the OAE-2 C-isotope excursion, pyrite δ^{34}S values are at their minimum, generally –30‰. In the upper part of the core (depths < 65 m), post-OAE, pyrite δ^{34}S values return to pre-excursion values (–5 to –10‰). Organic matter δ^{34}S values express a muted drop from near –2‰ to a minimum of –8.9‰ at the onset of OAE-2 and a gradual increase thereafter, reaching ~4‰ in the top of the section.

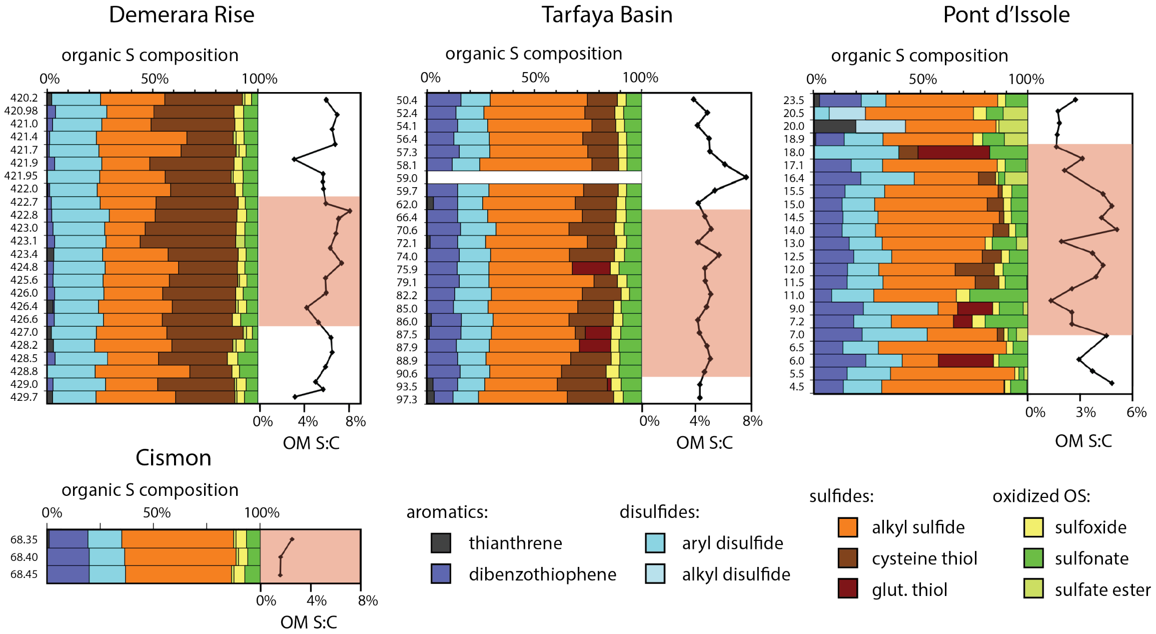

Fig. 6: Organic S speciation in organic matter. XAS and OM S:C (mol%) ratios show consistent organic S redox speciation among Demerara, Tarfaya, and Cismon samples and more variable speciation associated with local environmental change in Pont d'Issole. The

red shaded intervals correspond to the OAE-2 C-isotope excursion at each site. Categories of reduced S structures (aromatic, disulfide, and sulfide) can be confidently distinguished, but specific identifications within these groups (e.g., between sulfides and thiols) are tentative.

X-ray absorption spectroscopy was used to quantify the relative contributions of different forms of organic S to the total solvent- and acid-insoluble OM pool (Eglinton et al., 1994; Vairavamurthy, 1998). At Demerara Rise and Tarfaya Basin, the speciation of organic S is remarkably consistent before, during, and after the OAE-2 C-isotope excursion (Fig. 6), contrasting the variation observed in the Pont d'Issole profile (Fig. 6; Raven et al., 2018). Additionally, as summarized in Supplementary Table 1, the redox speciation of S-rich OM (S:C $\geq$ 3%) is quite comparable at all four sites, with over half of organic S present as alkyl sulfides and substantial amounts of disulfides and sulfonates. There are subtle, yet robust, site-to-site differences in organic S speciation, with Demerara Rise OM richer in disulfides and leaner in aromatic S forms than OM from Cismon, Tarfaya Basin, and Pont d'Issole shales. In less strongly sulfurized samples from Pont d'Issole, the relative proportions of oxidized organic S forms – sulfonates and sulfate esters – are generally higher at the expense of alkyl sulfides (Raven et al., 2018).

4. Discussion

4.1 Organic matter S:C ratios and local redox state

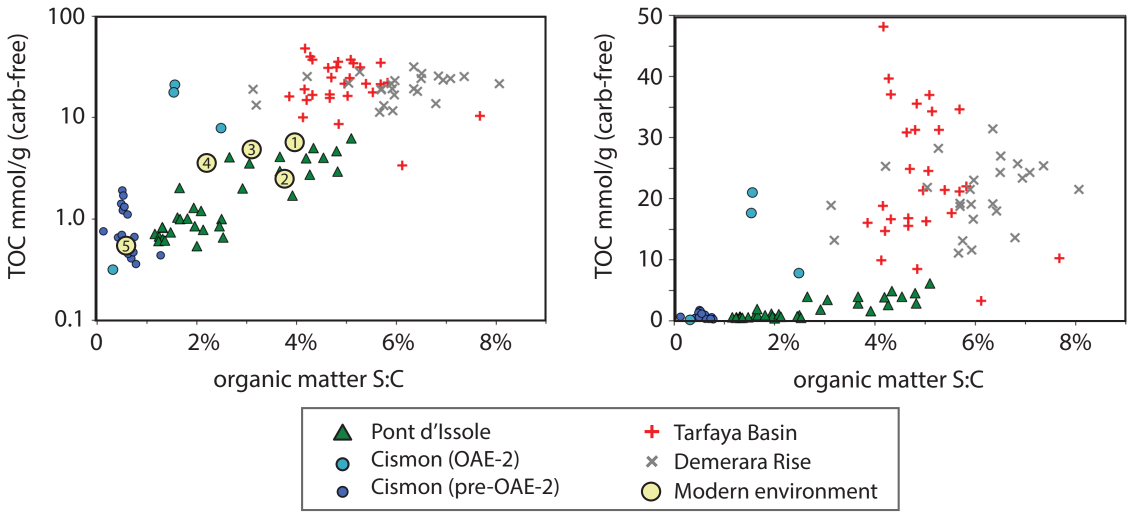

Fig. 7 Global relationship between sulfurization intensity and TOC preservation. Relationships between the intensity of sulfurization (molar S:C ratio) and TOC concentrations (mmol/g on a carbonate-free basis) are shown on log (left) and linear (right) scales; for versions of these plots on a whole-rock basis, see Supplementary Figure 1. Circled numbers on left panel refer to published values from modern environments: (1) Cariaco Basin sediments (Werne et al., 2003); (2) the Peru Margin (Eglinton et al., 1994); (3) the Namibian Margin (Dale et al., 2009); (4) Santa Barbara Basin sediments (Raven et al., 2016b); and (5) Gulf of Lion sediments (this study; Supplementary Table 2).

The S:C ratio of OM provides an indicator of the relative intensity of sulfurization reactions, with primary biomass values typically below 1 mol% and strongly sulfurized OM exceeding ~3 mol% (Francois, 1987). OM S:C ratios can also be used to infer the location of sulfurization (e.g., in particles sinking through the water column, at the sediment-water interface, or within the sediments), which is largely a function of the redox structure of the local depositional environment. Elevated OM S:C ratios require organic substrates with a high density of functional groups available to react with (poly)sulfide; we refer to these groups as functionally 'sulfurizable moieties,' recognizing that certain moieties may be conditionally sulfurizable, contingent on the chemical and physical properties of the environment (Blair and Aller, 2012). Still, we broadly expect the highest concentrations of sulfurizable moieties in surface water, where fresh marine OM is relatively rich in sulfurizable aldehydes, alcohols, and conjugated double bonds (Amrani and Aizenshtat, 2004). The concentration of these moieties in particulate OM will decrease with depth as microbial heterotrophs degrade and consume oxygen- and energy-rich components of the milieu like sugars and proteins (Hedges et al., 1999).

Figure 7 illustrates how the relationship between the S:C ratio and concentration of TOC for the four compiled OAE-2 sites compares with published data from modern environments with different redox conditions. Bottom waters from Cariaco Basin (labeled '1') are sulfidic below ~250 m water depth (Werne et al., 2003); bottom waters from the Peru ('2') and Namibian ('3') Margins are O_2-depleted but rarely sulfidic, with sulfidic sediments (Dale et al., 2009; Eglinton et al., 1994); bottom waters in Santa Barbara Basin ('4') are intermittently oxic, with sulfidic sediments; and both the bottom water and shallow sediments in the Gulf of Lion ('5') are oxic. Among these modern sites, S:C ratios and OM concentrations are highest in sediments from the sulfidic Cariaco Basin and lowest in sediments from the oxic Gulf of Lion. Of course, each of these sites is also affected by unique chemical and physical characteristics of the environment. For example, sedimentation rates are high on the Peru Margin due to the weathering of the Andes and the abundance of detrital silica from diatoms, both of which presumably dilute OM concentrations relative to other sites (Fig. 7). Despite this caveat, these modern sites conform to a trend toward higher S:C ratios and higher OM concentrations associated with increasingly O_2-limited environments.

The S:C ratios and TOC concentrations for modern sites overlap with the range of data from Pont d'Issole and Cismon (Fig. 7). At least in terms of these bulk parameters, OM-lean carbonate rocks from both sites resemble modern deposits from the oxic Gulf of Lion, and more TOC-rich shales from Pont d'Issole resemble more O_2-limited sites like the Peru Margin and Cariaco Basin. In a previous study that focused only on samples from Pont d'Issole, positive correlations among OM S:C ratios, TOC concentrations, and OM $\delta^{34}S$ values were attributed to changes in local redox conditions (Raven et al., 2018), consistent with these modern analogs. During more O_2-limited periods at Pont d'Issole, rapid OM sulfurization reactions likely generated OM with S:C ratios near 5% in the water column or near the sediment-water interface, where relatively fresh OM contains at least that concentration of functionally sulfurizable moieties. During more oxic periods, gradual sulfurization reactions in sediments affected older OM (≥10s of years) with a lower concentration of sulfurizable moieties and generated OM with S:C ratios closer to 2% (Raven et al., 2018).

Southern proto–North Atlantic OAE-2 samples extend the trend in Figure 7 toward even greater OM concentrations and S:C ratios than those associated with bottom water anoxia at Cismon, Pont d'Issole, and modern sites. We lack modern analogues for remarkable hotspots of TOC burial like Tarfaya Basin, which had an outsized role in driving changes in the OAE-2 C and S cycles (Kolonic et al., 2005; Sinninghe Damsté and Köster, 1998).

At both Demerara Rise and Tarfaya Basin, there is abundant evidence for water column euxinia and at least intermittent photic zone anoxia. Finely laminated sediments from Demerara Rise (Erbacher et al., 2005) contain only occasional benthic foraminifera (Friedrich et al., 2006), iron speciation documents local sulfidic conditions (Owens et al., 2016), and trace metals also suggest reducing local conditions (Hetzel et al., 2009) that expand globally during the event (Owens et al., 2016). At Tarfaya, an anoxic and commonly sulfidic water column is evidenced by iron speciation, organic petrography, and the presence of biomarkers for phototrophic sulfide oxidizing bacteria (in nearby core S13; Kuypers et al., 2002; Poulton et al., 2015). Still, there is also evidence for periodic, short-lived intervals of less strongly reducing conditions (Poulton et al., 2015), potentially contributing to slightly lower OM S:C ratios at this site than at Demerara. In general, however, reducing conditions at both southern proto–North Atlantic sites could have facilitated rapid, extensive sulfurization of a large pool of fresh OM in sinking particles with a high concentration of functionally sulfurizable moieties (Sinninghe Damsté and Köster, 1998). We emphasize that, in contrast with prior work, our conceptual model invokes near–instantaneous reactions between OM with some concentration of sulfurizable moieties and polysulfide, wherever sulfide and oxidants are first available in the environment. Polysulfide 'availability' for sulfurization will depend on microbial sulfate reduction rates, oxidant availability, and competition with Fe; importantly, however, it does not necessarily imply measurable free sulfide in the ('bulk') water column.

We can also compare OM from Demerara Rise and Tarfaya Basin with the results of laboratory sulfurization experiments utilizing fresh algal biomass or model compounds. In the presence of excess polysulfides, lipids and carbohydrates sulfurize to form macromolecular material in which characteristic components have S:C ratios around 2–3% (Gelin et al., 1998) and ~6.7% (van Dongen et al., 2003), respectively. For dissolved organic matter, bulk molar S:C ratios can apparently be much higher, reaching as much as 15% in recent experiments (Pohlabeln et al., 2017). Still, the average S:C ratios of (bulk, particulate) OM from Tarfaya Basin (5.0%), Demerara Rise (5.9%), and Cismon shales (5.0%) indicate that the OM sulfurizing in these environments had a concentration of sulfurizable moieties similar to the constituents of fresh, carbohydrate–rich algal biomass. Experimental data thus lend credence to the hypothesis that rapid, likely particle-hosted, sulfurization drove OM preservation in the water columns of both Tarfaya Basin and Demerara Rise.

Broadly speaking, the relationship between S:C ratio, OM preservation, and local redox structure appears to be generalizable for marine environments, with the highest S:C ratios and TOC concentrations supported by rapid, particle-hosted sulfurization under strongly O_2-limited conditions. The observation that OM sulfurization is an apparently major control on OM burial in diverse redox settings invites parameterization and application of this trend to models of carbon cycling on local to global scales and throughout the geologic record.

4.2 Interpreting organic matter and pyrite $\delta^{34}S$ records

To first order, the sulfur isotope compositions of pyrite and organic S reflect the $\delta^{34}S$ value of sulfide and/or polysulfide in the environment where that solid phase formed, with OM commonly ~5–10‰ more ^{34}S-enriched than coexisting pyrite (Anderson and Pratt, 1995). Accordingly, S–isotope ratios – of both pyrite and sulfurized OM – provide potentially powerful archives of information about the availability and distribution of sulfide in the environment. Several primary factors affect the integrated (poly)sulfide $\delta^{34}S$ value recorded in pyrite and OM, including (1) the $\delta^{34}S$ value of the sulfate used in microbial sulfate reduction (MSR, Fike and Grotzinger, 2008); (2) the fractionation factor associated with MSR (ε_{MSR}, Kaplan and Rittenberg, 1964); (3) the position of the chemocline relative to diffusively 'closed' sediments (Jorgensen, 1979) and (4) the concentration of sulfate and resulting depth of sulfate depletion (Adams et al., 2010). Importantly, all of these processes impact the distribution and/or $\delta^{34}S$ value of (poly)sulfide in the environment and should therefore impact the S-isotope composition of both pyrite and OM, generating roughly parallel $\delta^{34}S$ profiles. If pyrite and OM $\delta^{34}S$ profiles are not parallel, then we need to invoke processes that affect these sinks differently.

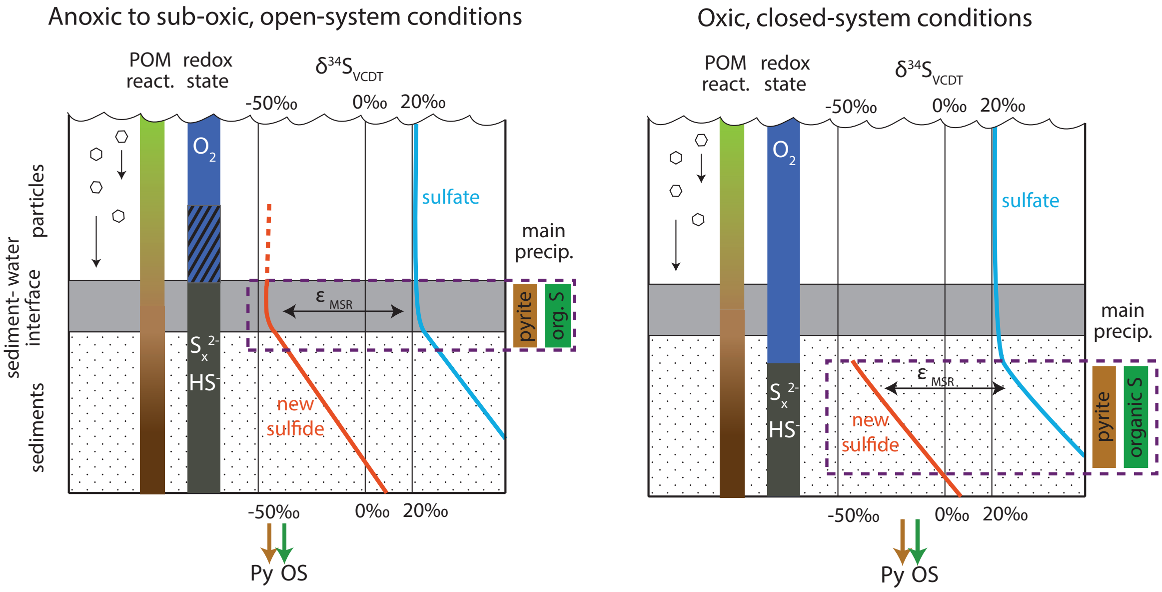

Fig. 8: Model for organic S and pyrite formation at Pont d’Issole and Cismon. The color scale labeled “POM react.” represents a generalized decline in the reactivity of particulate OM with age since export from the photic zone. At left, the dashed red line and hatched redox state depict differences between sub-oxic and anoxic conditions. Under anoxic conditions, the zone of precipitation for pyrite and organic S would move upward with the chemocline. Diagram is not to scale.

At Pont d’Issole, OM and pyrite δ^{34}S profiles move in roughly parallel between the TOC-rich and TOC-lean layers associated with OAE-2 (Fig. 2). Accordingly, these phases appear to be primarily recording changes in the δ^{34}S value or distribution of sulfide in the environment. Like OM δ^{34}S values at this site (Raven et al., 2018), pyrite δ^{34}S values describe the extent to which sulfate was diffusively limited in sediments, shown schematically in Fig. 8. Under conditions where O_2 concentrations are drawn down to zero at roughly the sediment-water interface (which we call ‘sub-oxic’ in Fig. 8), MSR in the shallowest sediments can access the open-ocean pool of seawater sulfate with an unfractionated δ^{34}S value, and the resulting strongly ^{34}S-depleted sulfide from MSR is recorded in both pyrite and OM. Under more 'oxic' conditions, O_2 penetrates deeper in the sediments and microbial sulfate reduction occurs in a diffusively sulfate–limited environment. As available sulfate is consumed with some fractionation (ε_{MSR}), residual sulfate in porewater becomes enriched in ^{34}S, and the organic and inorganic sulfur pools that precipitate within such a (partially) closed system have higher integrated δ^{34}S values than those formed in open systems. At Pont d'Issole, S–isotope evidence for more closed-system MSR is also associated with smaller amounts of preserved OM with a lower S:C ratio (Raven et al., 2018).

Both organic S and pyrite from Cismon black shales are strongly ^{34}S-depleted, consistent with generally open-system pyrite and organic S formation during the OAE C-isotope excursion. These low δ^{34}S values resemble S-isotope values observed in sediments from modern sulfidic basins, which have been attributed to open-system pyritization (Lyons et al., 2003). As noted by the dashed vertical red line in Fig. 8, the critical sulfidic environment(s) hosting these reactions could be very shallow sediments and/or particles sinking through the water column. In deeper carbonates from Cismon, OM is only weakly sulfurized (S:C averaging 0.6 mol%), so the connection between dissolved (poly)sulfides and the δ^{34}S value of OM is less robust. High $\Delta\delta^{34}S_{OS\text{-}pyrite}$ values for samples with low S:C ratios ($\leq$1.0 mol%) could reflect contributions from detrital, biomass, or macrofaunal exudate sources to organic S in addition to sulfurization.

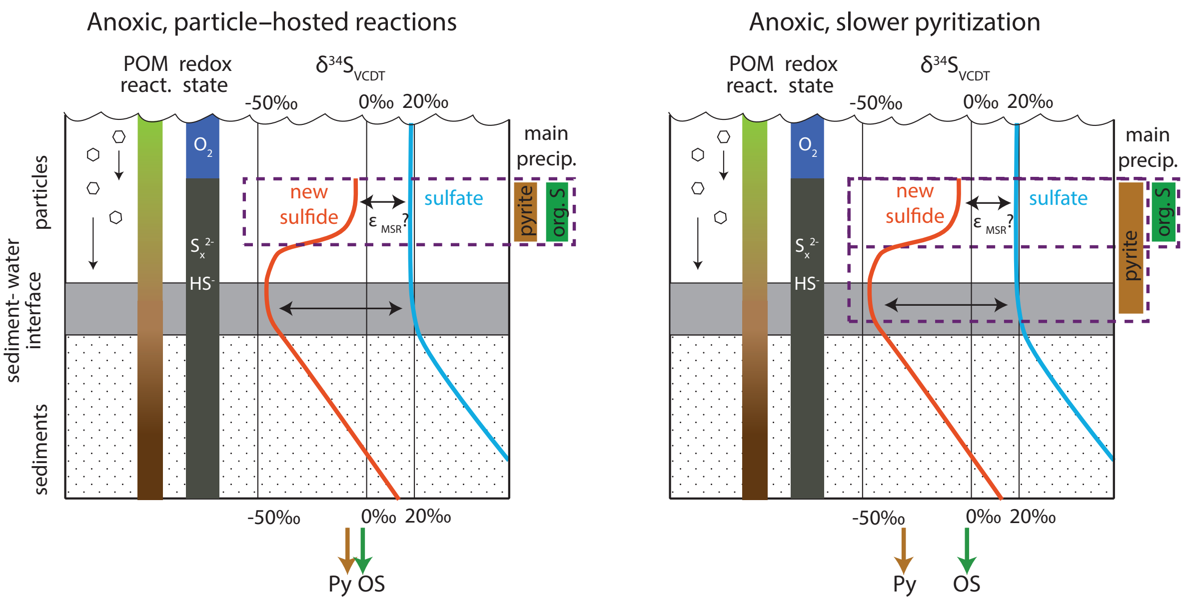

Fig. 9 Proposed model for OAE-2 δ^{34}S records at Tarfaya and Demerara. Left panel shows hypothesized conditions ≥190,000 yrs before the onset of OAE-2. Right panel shows a scenario for explaining pyrite and OM δ^{34}S values during the early part of the OAE-2 C-isotope excursion. Changes in available Fe could slow the rate of pyrite formation relative to OM sulfurization and generate more ^{34}S-depleted pyrite without impacting the S-isotope composition of OM. The color scale labeled "POM react." represents a generalized decline in the reactivity of particulate OM with age since export from the photic zone. Diagram is not to scale.

Different processes impact δ^{34}S patterns at Tarfaya Basin and Demerara Rise. A wealth of data supports the idea that the Tarfaya Basin and Demerara Rise water columns were typically euxinic before and after OAE-2, which would imply open-system S cycling that leads to ^{34}S-depleted pyrite and OM (Hetzel et al., 2009; Poulton et al., 2015). Yet, δ^{34}S values of pyrite and OM from both of these sites are near –5‰ at these times, much more ^{34}S-enriched than samples from other sites with open-system MSR. To reconcile these observations, we propose that the $\delta^{34}S$ values recorded in plentiful OM at Tarfaya Basin and Demerara Rise do reflect the S-isotope composition of sulfide in sinking particles, and that this sulfide was relatively ^{34}S-enriched (Fig. 9; below). Similarly, there is limited evidence for the existence of transiently ^{34}S-enriched sulfide in particles from Cariaco Basin during a period of peak productivity and sinking OM flux (Raven et al., 2016a). Particles from this period contain abundant C_{20} thiophene, a common sulfurized organosulfur compound, with a much more ^{34}S-enriched composition (–14.1 to 3.1‰) than during other times (–29.9 to –18.2‰), indicating at least the transient existence of relatively ^{34}S-enriched (poly)sulfide in particles (Raven et al., 2016a) despite deep basin sulfide $\delta^{34}S$ values near –30‰ (Li et al., 2010). The dramatic increase in inferred sulfide $\delta^{34}S$ values in particles from Cariaco Basin, Tarfaya Basin, and Demerara Rise (Fig. 9) contrasts with the slight (~5‰) increases in sulfide $\delta^{34}S$ value frequently observed in the uppermost portion of modern sulfidic water columns (Lyons et al., 2003), which are attributed to oxidative S-cycling microorganisms and/or abiotic sulfide oxidation. Thus, the $\delta^{34}S$ values of strongly sulfurized OM and pyrite in TOC-rich sediments may capture the signature of MSR occurring rapidly in sinking particles.

The large fluxes of fresh OM that reached O_2-limited parts of the environment in both Tarfaya Basin and Demerara Rise make these sites likely candidates for the operation of rapid, substrate-replete MSR, which could lead to relatively ^{34}S-enriched sulfide in particles via smaller isotope fractionations during sulfate reduction, sulfate drawdown within diffusively limited microenvironments, or both. The fractionation factor associated with MSR (ε_{MSR}) is highly variable and depends broadly on MSR rate (Kaplan and

Rittenberg, 1964). Although most marine systems have apparent S-isotope fractionation factors closer to the equilibrium fractionation between sulfate and sulfide of 72‰, low ε_{MSR} values (<25‰) are associated with high rates of cell-specific MSR, on the order of >25 fmol H_2S/cell/day (Wenk et al., 2017), observed for sulfate reducers in laboratory settings with plentiful carbon substrates and nutrients. These "small" S-isotope fractionations are consistent with the 20–30‰ difference between seawater sulfate (at ~19‰) and apparent particle-hosted sulfide observed at Tarfaya Basin and Demerara Rise. Alternatively or in addition to changes in ε_{MSR}, if particles are sufficiently large (>> 1 mm), it is possible for sulfate to become diffusively limited within particle microenvironments (Louca and Crowe, 2017), especially given relatively low seawater sulfate concentrations at this time (Lowenstein et al., 2003; Owens et al., 2013; Gomes et al., 2016). Very high rates of MSR could therefore drive the remaining sulfate pool within microenvironments toward higher $\delta^{34}S$ values and contribute to relatively ^{34}S-enriched sulfide.

The alternative explanation for our results attributes the relatively ^{34}S-enriched composition of pyrite and OM at Tarfaya Basin and Demerara Rise prior to the onset of the OAE to their formation from sediment porewater. Importantly, it also requires that these phases form semi-continuously during burial to the depths at which sulfate is nearly fully drawn down, to integrate to bulk compositions near –5‰. Barring extreme sedimentation events, this implies maximum OM sulfurization rates on the timescales of at least tens to hundreds of years – sufficient to accumulate a diffusively limiting layer – not the days to weeks observed in Cariaco particles and laboratory experiments. Additionally, this explanation for Tarfaya Basin and Demerara Rise $\delta^{34}S$ patterns is difficult to reconcile with the S:C ratio of OM. For OM to incorporate up to 6 mol% S gradually over at least years of aging, that OM must have retained a high density of sulfurizable moieties that were somehow also effectively inaccessible to heterotrophs. Theoretically, this could result from enhanced preservation mechanisms other than sulfurization, notably physical protection by association with clays or other mineral surfaces (Hedges and Keil, 1995) or the absence of bioturbating macrofauna (Middelburg and Levin, 2009). Still, the sheer abundance of OM in Tarfaya Basin and Demerara Rise sediments would overwhelm available clays, and it is difficult to envision a mechanism to sulfurize OM after many years of effective physical protection. We therefore consider a purely closed-system sedimentary origin for the moderately ^{34}S-enriched OM at Tarfaya Basin and Demerara Rise improbable.

Similar to OM throughout the section, pyrite in the lowest part of the section at both Tarfaya Basin and Demerara Rise has relatively high δ^{34}S values. Under these pre-OAE-2 conditions, the offset between pyrite and OM δ^{34}S values is 5–10‰, similar to the offset observed in other environments that are thought to host open-system concurrent pyritization and OM sulfurization (Cariaco Basin, Cismon). Starting significantly before the onset of OAE-2, pyrite δ^{34}S begins to move independently of OM δ^{34}S, increasing $\Delta\delta^{34}S_{OS\text{-}py}$ values. Little-to-no concurrent shift is seen in the OM δ^{34}S record. Similarly, XAS data show a lack of change in the speciation of organic S across the onset of OAE-2 at both Tarfaya Basin and Demerara Rise (Fig. 5), suggesting consistent conditions for OM sulfurization throughout. Therefore, the shift in pyrite δ^{34}S values is caused by a process that impacts the kinetics of one sulfide sink relative to the other, not by a change in sulfide distribution or ε_{MSR} in the environment. In the case of pyrite at the onset of OAE-2 at

Tarfaya and Demerara Rise, the observed shift indicates that the zone of pyrite formation expanded into deeper portions of the water column and/or sediment, integrating more ^{34}S-depleted sulfide generated from MSR at more typical (slow) environmental rates (Fig. 9) for reasons we discuss below.

4.3 Global pyrite δ^{34}S patterns and OAE-2 implications

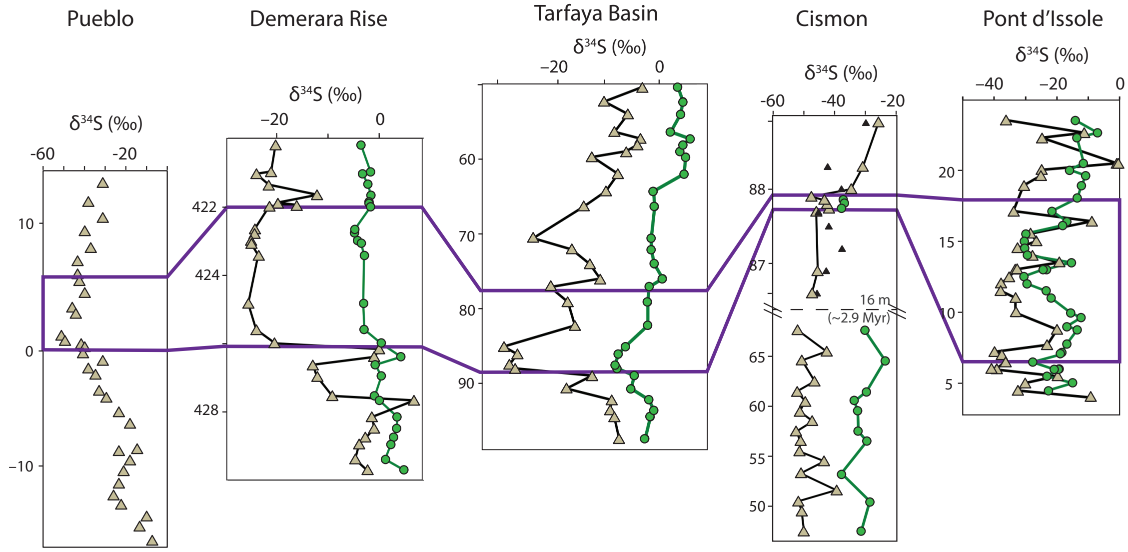

Fig. 10 Summary of δ^{34}S records across OAE-2. Green circles show OM δ^{34}S values and brown triangles show pyrite δ^{34}S values. Pueblo data are from Adams et al. (2010). The gap in the Cismon y-axis represents 16 m of TOC-lean carbonates (~2.9 Myr), and small black triangles are previously published pyrite (CRS) data (Gomes et al., 2016). The C-isotope excursion, representing an estimated 500 kyr of accumulation, is outlined in purple. Pyrites from Demerara Rise, Tarfaya Basin, and Pueblo all become more ^{34}S-depleted leading up to the onset of OAE-2.

The decrease in pyrite $\delta^{34}S$ values prior to the onset of OAE-2 appears to be a widespread phenomenon, with remarkably similar profiles from Demerara Rise, Tarfaya Basin, and the Western Interior Seaway (Pueblo; Adams et al., 2010). Because the ~20‰ negative $\delta^{34}S$ shift in pyrite at Tarfaya and Demerara is not observed in the $\delta^{34}S$ profile of OM, it is not likely to primarily reflect changes in the spatial distribution or $\delta^{34}S$ of dissolved sulfide in the environment. Instead, we propose that pyrite $\delta^{34}S$ patterns record changes in marine iron supply across OAE-2, which impacted the kinetics of pyrite precipitation and extended the zone of pyrite precipitation deeper in the sedimentary profile.

The highly reactive iron available for pyritization in marine environments is sourced from a mixture of detrital iron from the continents, hydrothermal iron from spreading ridges, and remobilized iron from biogeochemical cycling in shelf sediments (Poulton and Raiswell, 2002). Most sediments from the southern proto–North Atlantic during OAE-2 have elevated Fe_T/Al ratios (>0.5, the crustal average value) and near–zero $\delta^{56}Fe$ compositions, suggesting that a significant component of the iron delivered to these sites was from hydrothermal sources (Owens et al., 2012). The processes that facilitate the transport of hydrothermally sourced iron remain subjects of active research, but appear to involve stabilization of Fe^{3+} in colloidal or nanoparticulate phases (Fitzsimmons et al., 2017). Hydrothermal iron that encounters dissolved sulfide can precipitate as an Fe-sulfide and be trapped in place as pyrite, restricting the amount of iron that can be transported through euxinic basins to distal sites. In contrast, iron is highly mobile in anoxic but non-sulfidic seawater. The delivery of iron to Demerara Rise and Tarfaya Basin was therefore likely sensitive to the redox state of nearby environments, and hydrothermal iron delivery could have been significantly curtailed by nearby euxinia.

In addition to impacting the total flux of iron transported throughout the basin, expanding anoxia is likely to affect its mineralogy. The source of Fe for pyritization is commonly presumed to be dissolved Fe^{2+}, which can be released from Fe^{III}-bearing minerals by reduction either abiotically with bisulfide (Canfield, 1989) or biotically by Fe-reducing microorganisms. The rates of both types of iron reduction vary depending on the mineralogy and specific surface area of the Fe^{III} involved: poorly crystalline oxyhydroxides like ferrihydrite and lepidocrocite are reduced within hours to days, while crystalline oxides and oxyhydroxides like goethite and hematite are reduced more slowly, and Fe-bearing silicates can persist for millennia (Poulton and Canfield, 2005; Raiswell and Canfield, 1996). Where concentrations of Fe^{2+} and sulfide in solution are sufficiently high, pyrite precipitation is generally thought to proceed via precipitation of an iron monosulfide intermediate that subsequently converts to pyrite. Intriguingly, Wan et al. (2017) recently described a second category of pyritization mechanism with the potential to drive pyrite formation where Fe^{III}–oxide surfaces are plentiful and vastly exceed the available HS^-. Under these conditions, ferric hydroxide surfaces can mediate the rapid nucleation of pyrite via the formation of $>Fe^{II}S_2^-$, making redox interfaces and sinking particles with high Fe^{III}:HS^- ratios potential hotspots for surface-mediated pyritization of ferric hydroxides. Expanding regional euxinia would likely reduce the transport of ferric hydroxides to euxinic sites like Demerara Rise and Tarfaya Basin, lowering the Fe^{III}:HS^- ratio near critical interfaces in the water column. The resulting change in the relative importance of surface-mediated versus dissolved-phase pyritization mechanisms could thus contribute to the observed shift in pyrite $\delta^{34}S$. Regardless of the significance of this particular mechanism, changing regional redox could impact the mineralogy of remobilized Fe more broadly by changing the rates and/or environmental conditions of (oxy)hydroxide formation during repetitive redox cycling, generating a different suite of Fe^{III} minerals that re-release Fe^{2+} into the depositional environment at diverse rates. The bulk pyrite $\delta^{34}S$ records we present here reflect the integrated pool of pyrite derived from precipitation on multiple timescales following Fe^{III}–mineral (re-)reduction as well as potentially from ferric hydroxide surface–mediated reactions. Separating these various contributors to bulk pyrite records will be essential for understanding how expanding regional anoxia and euxinia impacted the abundance and mineralogy of iron sources and, by extension, the kinetics of pyritization.

Trace metal concentrations and thallium isotopes from Demerara Rise provide evidence for the expansion of regional to more global anoxia prior to the onset of the OAE-2 C-isotope excursion (Ostrander et al., 2017; Owens et al., 2016). Like iron, the redox-sensitive elements Zn, V, and Mo are readily sequestered in anoxic and/or sulfidic sediments, and this process is thought to be responsible for their apparent removal from seawater prior to OAE-2 (Owens et al., 2016). Using an extrapolation of the estimated OAE-2 linear sedimentation rate (0.8 cm/kyr) to 427.5 m, pyrite $\delta^{34}S$ values at Demerara begin to decrease ~190 kyr before the onset of OAE-2. This depth corresponds to the initial drop in concentrations of Zn in this core, a sensitive indicator of anoxia with a short residence time (~11 kyr, Little et al., 2014) that implies a global increase in non-sulfidic, anoxic conditions significantly before the onset of OAE-2. The decrease in pyrite $\delta^{34}S$ values is complete by the onset of the OAE, in sediments evidencing drawdown of even sulfide-sensitive Mo, indicating prevalent sulfidic environments (Owens et al., 2016). The gradual pre-OAE pyrite $\delta^{34}S$ shift at Demerara thus corresponds to a period of intensification of regional to global anoxia prior to the OAE and an expansion of sulfidic conditions globally (Owens et al., 2013).

Changes in the delivery of iron to sites in the southern proto–North Atlantic could have generated the shift in pyrite $\delta^{34}S$ that we observe by slowing the kinetics of pyrite formation. For example, if the combination of expanding euxinia and volcanic activity caused the main source of Fe at these sites to switch from more hydrothermally sourced, organic–complexed Fe^{III} to detrital or volcanic crystalline oxy-hydroxides, the rate of Fe^{2+} release to solution in sinking marine particles could have dropped dramatically. The conceptual model put forth in Fig. 9 predicts that this scenario would yield more ^{34}S-depleted pyrite overall. Importantly, this could occur while the total quantity of pyrite eventually buried remained nearly constant.

At Pueblo and Tarfaya Basin, the onset of the shift toward more ^{34}S-depleted pyrite is staggered relative to Demerara Rise (Fig. 10). Using published interpolated Ar-Ar ages from ammonite biozones, pyrite $\delta^{34}S$ values at Pueblo drop in two stages at ~400 kyr and ~200 kyr before the onset of OAE-2 (Adams et al., 2010). At Tarfaya Basin, if we extrapolate estimated OAE-2 accumulation rates (3.3 cm/kyr) similar to Demerara, then the pyrite $\delta^{34}S$ shift occurs ~82 kyr before the OAE. Osmium, strontium, and other geochemical proxies indicate regional heterogeneity in hydrothermal activity in different ocean basins at this time (du Vivier et al., 2014), which would also impact hydrothermal iron fluxes (Owens et al., 2012). Importantly, the Western Interior Seaway has a different redox structure leading up to OAE-2 than the rest of the proto-North Atlantic and Tethys, which likely leads to differences in the history of iron cycling among these sites.

Records from OAE-2 exemplify how the timing and location of pyritization can be affected by changes in iron supply in addition to changes in sulfur cycling. They also suggest that organic S should be incorporated into future models for the S cycle for OAEs. For example, because organic S is more typically more ^{34}S-enriched than pyrite, previous estimates for the extent of euxinia during OAE-2 based on S-isotope mass balance (e.g., Owens et al., 2013) may be conservative. OM sulfurization could have been an important factor for driving high organic carbon mass accumulation rates even for localities with low TOC (Owens et al., 2018), supporting massive global OM burial. By investigating the S-isotope behavior of both pyrite and OM, we can begin to take full advantage of these complex and powerful archives.

5. Conclusions

Rapid, particle-hosted OM sulfurization may have been a central process facilitating enhanced OM preservation across large swaths of the Tethys and North Atlantic Oceans before, during, and after OAE-2. Explicit consideration of rapid OM sulfurization in O_2-limited environments thus has the potential to improve models of TOC preservation and remineralization in both modern and ancient systems.

Paired OM and pyrite δ^{34}S profiles make it possible to disentangle the effects of chemocline position, sulfate reduction rate, and regional-to-global geochemical perturbations on S-isotopes in the rock record. In the several hundred thousand years leading up to the onset of OAE-2, pyrite and OM δ^{34}S records indicate a globally widespread change in the timing of pyrite formation relative to OM sulfurization, which both S-isotope and speciation (XAS) data argue occurred consistently across this interval. A regional expansion of euxinic conditions and changes in volcanic activity may have contributed to changes in the speciation of iron available for pyritization and thus to the relatively slow formation of relatively ^{34}S-depleted pyrite during the OAE. This change in global iron cycling could not be identified from pyrite δ^{34}S profiles alone, underscoring the value and untapped potential of paired pyrite – OM S-isotope records for exploring the geologic record.

Acknowledgements

We are grateful for financial support to M.R.R. from the Agouron Institute (Geobiology Post-doctoral Fellowship) and to Itay Halevy (Weizmann Institute, Israel), Matt Hurtgen, and Brad Sageman (Northwestern University, USA) for valuable discussions. Melanie Suess, Jen Houghton, and Stephanie Moore provided technical support for analyses at Washington University in St. Louis. Tarfaya and Demerara samples were obtained via Wolfgang Kuhnt (Kiel University) and IODP, respectively. Virgil Pasquier (Weizmann Institute, Israel) provided Gulf of Lion samples. JDO would like to acknowledge support from NASA Exobiology (80NSSC18K1532). This work was enhanced by XAS analyses at the Stanford Synchrotron Radiation Laboratory under User Proposal 4885, as well as by the efforts of SSRL staff. Use of the Stanford Synchrotron Radiation Lightsource, SLAC National Accelerator Laboratory, is supported by the U.S. Department of Energy, Office of Science, Office of Basic Energy Sciences under Contract No. DE-AC02-76SF00515.

Supplemental Information:

Fig. S1: whole-rock basis version of Fig. 6

Table S1: Average relative abundances of organic S moieties for sections spanning OAE-2 by XAS

Table S2: Gulf of Lion average composition

Table S3: Compiled geochemical results

Table S4: Compiled XAS results

References

Adams, D.D., Hurtgen, M.T., Sageman, B.B., 2010. Volcanic triggering of a biogeochemical cascade during Oceanic Anoxic Event 2. Nature Geoscience 3, 201–204.

Amrani, A., Aizenshtat, Z., 2004. Mechanisms of sulfur introduction chemically controlled: δ34S imprint. Organic Geochemistry 35, 1319–1336. doi:10.1016/j.orggeochem.2004.06.019

Anderson, T.F., Pratt, L.M., 1995. Isotopic evidence for the origin of organic sulfur and elemental sulfur in marine sediments. In: Geochemical Transformations of Sedimentary Sulfur. ACS Symposium Series, vol. 612, 378–396. American Chemical Society, Washington DC.

Bellanca, A., Claps, M., Erba, E., Masetti, D., Neri, R., 1996. Orbitally induced limestone/marlstone rhythms in the Albian—Cenomanian Cismon section (Venetian region, northern Italy): Sedimentology, calcareous and siliceous plankton distribution, elemental and isotope geochemistry. Palaeogeography 126, 227–260. doi:10.1016/S0031-0182(96)00041-7

Blair, N.E., Aller, R.C., 2012. The Fate of Terrestrial Organic Carbon in the Marine Environment. Annu. Rev. Mar. Sci. 4, 401–423.

Boussafir, M., Gelin, F., Lallier-Verges, E., Derenne, S., Bertrand, P., Largeau, C., 1995. Electron microscopy and pyrolysis of kerogens from the Kimmeridge Clay Formation, UK: Source organisms, preservation processes, and origin of microcycles. Geochimica et Cosmochimica Acta 59, 3731–3747.

Canfield, D.E., 1989. Reactive iron in marine sediments. Geochimica et Cosmochimica Acta 53, 619–632. doi:10.1016/0016-7037(89)90005-7

Canfield, D.E., Raiswell, R., Westrich, J.T., Reaves, C.M., 1986. The use of chromium reduction in the analysis of reduced inorganic sulfur in sediments and shales. Chemical Geology 54, 149–155.

Dale, A.W., Bruchert, V., Alperin, M., Regnier, P., 2009. An integrated sulfur isotope model for Namibian shelf sediments. Geochimica et Cosmochimica Acta 73, 1924–1944. doi:10.1016/j.gca.2008.12.015

du Vivier, A.D.C., Selby, D., Sageman, B.B., Jarvis, I., Gröcke, D.R., Voigt, S., 2014. Marine 187Os/188Os isotope stratigraphy reveals the interaction of volcanism and ocean circulation during Oceanic Anoxic Event 2. Earth and Planetary Science Letters 389, 23–33. doi:10.1016/j.epsl.2013.12.024

Eglinton, T.I., Irvine, J.E., Vairavamurthy, A., Zhou, W., Manowitz, B., 1994. Formation and diagenesis of macromolecular organic sulfur in Peru margin sediments. Organic Geochemistry 22, 781–799. doi:10.1016/0146-6380(94)90139-2

Erbacher, J., Friedrich, O., Wilson, P.A., Birch, H., Mutterlose, J., 2005. Stable organic carbon isotope stratigraphy across Oceanic Anoxic Event 2 of Demerara Rise, western tropical Atlantic. Geochemistry Geophysics Geosystems 6, 714–9. doi:10.1029/2004GC000850

Fike, D.A., Grotzinger, J.P., 2008. A paired sulfate–pyrite δ34S approach to understanding the evolution of the Ediacaran–Cambrian sulfur cycle. Geochimica et Cosmochimica Acta 72, 2636–2648. doi:10.1016/j.gca.2008.03.021

Fitzsimmons, J.N., John, S.G., Marsay, C.M., Hoffman, C.L., Nicholas, S.L., Toner, B.M., German, C.R., Sherrell, R.M., 2017. Iron persistence in a distal hydrothermal plume supported by dissolved–particulate exchange. Nature Geosci 10, 195–201. doi:10.1038/ngeo2900

Francois, R. (1987). A study of sulphur enrichment in the humic fraction of marine sediments during early diagenesis. Geochimica Et Cosmochimica Acta, 51, 17–27.

Friedrich, O., Erbacher, J., Wilson, P. A., Moriya, K., & Mutterlose, J. (2009). Paleoenvironmental changes across the Mid Cenomanian Event in the tropical Atlantic Ocean (Demerara Rise, ODP Leg 207) inferred from benthic foraminiferal assemblages. Marine Micropaleontology, 71(1-2), 28–40. http://doi.org/10.1016/j.marmicro.2009.01.002

Gambacorta, G., Jenkyns, H.C., Russo, F., Tsikos, H., Wilson, P.A., Faucher, G., Erba, E., 2015. Carbon- and oxygen-isotope records of mid-Cretaceous Tethyan pelagic sequences from the Umbria – Marche and Belluno Basins (Italy). Newsl. Stratigr. 48, 299–323. doi:10.1127/nos/2015/0066

Gelin, F., Kok, M.D., De Leeuw, J.W., Sinninghe Damsté, J.S., 1998. Laboratory sulfurisation of the marine microalga Nannochloropsis salina. Organic Geochemistry 29, 1837–1848.

Gomes, M.L., Hurtgen, M.T., Sageman, B.B., 2016. Biogeochemical sulfur cycling during Cretaceous oceanic anoxic events: A comparison of OAE1a and OAE2. Paleoceanography 1–19. doi:10.1002/(ISSN)1944-9186

Hedges, J., & Keil, R. (1995). Sedimentary organic matter preservation: an assessment and speculative synthesis. Marine Chemistry, 49, 81–115.

Hedges, J.I., Hu, F.S., Devol, A.H., Hartnett, H.E., Tsamakis, E., Keil, R.G., 1999. Sedimentary organic matter preservation; a test for selective degradation under oxic conditions. American Journal of Science 299, 529–555.

Hetzel, A., Böttcher, M.E., Wortmann, U.G., Brumsack, H.-J., 2009. Paleo-redox conditions during OAE 2 reflected in Demerara Rise sediment geochemistry (ODP Leg 207). Palaeogeography, Palaeoclimatology, Palaeoecology 273, 302–328. doi:10.1016/j.palaeo.2008.11.005

Jarvis, I., Lignum, J.S., Gröcke, D.R., Jenkyns, H.C., 2011. Black shale deposition, atmospheric CO2 drawdown, and cooling during the Cenomanian-Turonian Oceanic Anoxic Event. Paleoceanography 26. doi:10.1029/2010PA002081

Jorgensen, B.B., 1979. A theoretical model of the stable sulfur isotope distribution in marine sediments. Geochimica et Cosmochimica Acta 43, 363–374.

Kaplan, I.R., Rittenberg, S.C., 1964. Microbiological fractionation of sulphur isotopes. Journal of General Microbiology 34, 195–212.

Keller, G., Adatte, T., Berner, Z., Chellai, E.H., Stueben, D., 2008. Oceanic events and biotic effects of the Cenomanian-Turonian anoxic event, Tarfaya Basin, Morocco. Cretaceous Research 29, 976–994. doi:10.1016/j.cretres.2008.05.020

Kolonic, S., Damsté, J., Böttcher, M.E., Kuypers, M.M.M., Kuhnt, W., Scheeder, G., Wagner, T., beckmann, B., 2002. Geochemical characterization of Cenomanian/Turonian black shales from the Tarfaya Basin (SW Morocco). Journal of Petroleum Geology 25, 325–350.

Kolonic, S., Wagner, T., Forster, A., Sinninghe Damsté, J.S., Walsworth-Bell, B., Erba, E., Turgeon, S., Brumsack, H.-J., Chellai, E.H., Tsikos, H., Kuhnt, W., Kuypers, M.M.M., 2005. Black shale deposition on the northwest African Shelf during the Cenomanian/Turonian oceanic anoxic event: Climate coupling and global organic carbon burial. Paleoceanography 20, 1–18. doi:10.1029/2003PA000950

Kuypers, M.M.M., Pancost, R.D., Nijenhuis, I.A., Sinninghe Damsté, J.S., 2002. Enhanced productivity led to increased organic carbon burial in the euxinic North Atlantic basin during the late Cenomanian oceanic anoxic event. Paleoceanography 17, 1–13. doi:10.1029/2000PA000569

Li, X., Gilhooly, W.P., III, Zerkle, A.L., Lyons, T.W., Farquhar, J., Werne, J.P., Varela, R., Scranton, M.I., 2010. Stable sulfur isotopes in the water column of the Cariaco Basin. Geochimica et Cosmochimica Acta 74, 6764–6778. doi:10.1016/j.gca.2010.08.020

Little, S.H., Vance, D., Walker-Brown, C., Landing, W.M., 2014. The oceanic mass balance of copper and zinc isotopes, investigated by analysis of their inputs, and outputs to ferromanganese oxide sediments. Geochimica et Cosmochimica Acta 125, 673–693. doi:10.1016/j.gca.2013.07.046

Louca, S., Crowe, S.A., 2017. Microscale reservoir effects on microbial sulfur isotope fractionation. Geochimica et Cosmochimica Acta 203, 117–139. doi:10.1016/j.gca.2017.01.007

Lowenstein, T.K., Hardie, L.A., Timofeeff, M.N., Demicco, R.V., 2003. Secular variation in seawater chemistry and the origin of calcium chloride basinal brines. Geology 31, 857–860. doi:10.1130/G19728R.1

Lyons, T.W., Werne, J.P., Hollander, D.J., Murray, R.W., 2003. Contrasting sulfur geochemistry and Fe/Al and Mo/Al ratios across the last oxic-to-anoxic transition in the Cariaco Basin, Venezuela. Chemical Geology 195, 131–157. doi:10.1016/S0009-2541(02)00392-3

Middelburg, J.J., Levin, L.A., 2009. Coastal hypoxia and sediment biogeochemistry. Biogeosciences 6, 1273–1293. doi:10.5194/bg-6-1273-2009

Ostrander, C.M., Owens, J.D., Nielsen, S.G., 2017. Constraining the rate of oceanic deoxygenation leading up to a Cretaceous Oceanic Anoxic Event (OAE-2: ~94 Ma). Science Advances 3, 1–6.

Owens, J.D., Gill, B.C., Jenkyns, H.C., 2013. Sulfur isotopes track the global extent and dynamics of euxinia during Cretaceous Oceanic Anoxic Event 2. Proceedings of the National Academy of Sciences 110, 18407-18412.

Owens, J.D., Lyons, T.W., Li, X., Macleod, K.G., 2012. Iron isotope and trace metal records of iron cycling in the proto North Atlantic during the Cenomanian Turonian oceanic anoxic event (OAE 2). Paleoceanography. doi:10.1029/2012PA002328

Owens, J.D., Lyons, T.W., Lowery, C.M., 2018. Quantifying the missing sink for global organic carbon burial during a Cretaceous oceanic anoxic event. Earth and Planetary Science Letters 499, 83–94. doi:10.1016/j.epsl.2018.07.021

Owens, J.D., Reinhard, C.T., Rohrssen, M., Love, G.D., Lyons, T.W., 2016. Empirical links between trace metal cycling and marine microbial ecology during a large perturbation to Earth's carbon cycle. Earth and Planetary Science Letters 449, 407–417. doi:10.1016/j.epsl.2016.05.046

Pohlabeln, A.M., Gomez-Saez, G.V., Noriega-Ortega, B.E., Dittmar, T., 2017. Experimental Evidence for Abiotic Sulfurization of Marine Dissolved Organic Matter. Frontiers in Marine Sci. 4, 265. doi:10.3389/fmars.2017.00364

Poulton, S., Canfield, D., 2005. Development of a sequential extraction procedure for iron: implications for iron partitioning in continentally derived particulates. Chemical Geology 214, 209–221. doi:10.1016/j.chemgeo.2004.09.003

Poulton, S.W., Henkel, S., März, C., Urquhart, H., Flögel, S., Kasten, S., Sinninghe Damsté, J.S., Wagner, T., 2015. A continental-weathering control on orbitally driven redox-nutrient cycling during Cretaceous Oceanic Anoxic Event 2. Geology 43, 963–966. doi:10.1130/G36837.1

Poulton, S.W., Raiswell, R., 2002. The low-temperature geochemical cycle of iron: From continental fluxes to marine sediment deposition. American Journal of Science 302, 774–805. doi:10.2475/ajs.302.9.774

Raiswell, R., Canfield, D.E., 1996. Rates of reaction between silicate iron and dissolved sulfide in Peru Margin sediments. Geochimica et Cosmochimica Acta 60, 2777–2787.

Raven, M.R., Fike, D.A., Gomes, M.L., Webb, S.M., Bradley, A.S., McClelland, H.-L.O., 2018. Organic carbon burial during OAE2 driven by changes in the locus of organic matter sulfurization. Nature Communications 9, 3409. doi:10.1038/s41467-018-05943-6

Raven, M.R., Sessions, A.L., Adkins, J.F., Thunell, R.C., 2016a. Rapid organic matter sulfurization in sinking particles from the Cariaco Basin water column. Geochimica et Cosmochimica Acta 190, 175–190. doi:10.1016/j.gca.2016.06.030

Raven, M.R., Sessions, A.L., Fischer, W.W., Adkins, J.F., 2016b. Sedimentary pyrite δ 34 S differs from porewater sulfide in Santa Barbara Basin: Proposed role of organic sulfur. Geochimica et Cosmochimica Acta 186, 120–134. doi:10.1016/j.gca.2016.04.037

Sageman, B.B., Meyers, S.R., Arthur, M.A., 2006. Orbital time scale and new C-isotope record for Cenomanian-Turonian boundary stratotype. Geology 34, 125–4. doi:10.1130/G22074.1

Sinninghe Damsté, J.S., Köster, J., 1998. A euxinic southern North Atlantic Ocean during the Cenomanian/Turonian oceanic anoxic event. Geochimica et Cosmochimica Acta 158, 165–173.

Vairavamurthy, A., 1998. Using X-ray absorption to probe sulfur oxidation states in complex molecules. Spectrochimica Acta Part A 54, 2009–2017. doi:10.1016/S1386-1425(98)00153-X

van Dongen, B.E., Schouten, S., Baas, M., Geenevasen, J.A.J., Sinninghe Damsté, J.S., 2003. An experimental study of the low-temperature sulfurization of carbohydrates. Organic Geochemistry 34, 1129–1144. doi:10.1016/S0146-6380(03)00060-3

Wan, M., Schröder, C., Peiffer, S., 2017. Fe (III): S (-II) Concentration Ratio Controls the Pathway and the Kinetics of Pyrite Formation during Sulfidation of Ferric Hydroxides. Geochimica et Cosmochimica Acta. doi:10.1016/j.gca.2017.08.036

Webb, S.M., 2005. SIXpack: a graphical user interface for XAS analysis using IFEFFIT. Phys. Scr. 2005, 1011. doi:10.1238/Physica.Topical.115a01011

Wenk, C.B., Wing, B.A., Halevy, I., 2017. Electron carriers in microbial sulfate reduction inferred from experimental and environmental sulfur isotope fractionations. The ISME Journal 12, 1–13. doi:10.1038/ismej.2017.185

Werne, J., Lyons, T., Hollander, D., Schouten, S., Hopmans, E., & Damste, J. (2008). Investigating pathways of diagenetic organic matter sulfurization using compound-specific sulfur isotope analysis. Geochimica Et Cosmochimica Acta, 72, 3489–3502.

Werne, J.P., Lyons, T.W., Hollander, D.J., Chemical, M.F., Sinninghe Damsté, J.S., 2003. Reduced sulfur in euxinic sediments of the Cariaco Basin: sulfur isotope constraints on organic sulfur formation. Geochimica et Cosmochimica Acta 195, 159–179. doi:10.1016/S0009-2541(02)00393-5